Biochimica et Biophysica Acta 1818 (2012) 2175–2183

Contents lists available at SciVerse ScienceDirect

Biochimica et Biophysica Acta

journal homepage: www.elsevier.com/locate/bbamem

Interaction of GAPR-1 with lipid bilayers is regulated by alternative homodimerization

Josse van Galen [a,1,2], Nick K. Olrichs [a,2], Arie Schouten [b], Ramon L. Serrano [a,3], Esther N.M. Nolte-'t Hoen [a], Ruud Eerland [a], Dora Kaloyanova [a], Piet Gros [b], J. Bernd Helms [a,*]

[a] Department of Biochemistry and Cell Biology and Institute of Biomembranes, Utrecht University, PO Box 80176, 3508 TD Utrecht, The Netherlands
[b] Crystal and Structural Chemistry, Bijvoet Center for Biomolecular Research, Faculty of Science, Utrecht University, Padualaan 8, 3584 CH Utrecht, The Netherlands

ARTICLE INFO

Article history:
Received 8 January 2012
Received in revised form 22 March 2012
Accepted 20 April 2012
Available online 26 April 2012

Keywords:
GAPR-1
GLIPR-2
Phytic acid
Dimerization
Protein–lipid interaction
Crystal structure

ABSTRACT

Golgi-Associated Plant Pathogenesis-Related protein 1 (GAPR-1) is a mammalian protein that belongs to the superfamily of plant pathogenesis related proteins group 1 (PR-1). GAPR-1 is a peripheral membrane-binding protein that strongly associates with lipid-enriched microdomains at the cytosolic leaflet of Golgi membranes. Little is known about the mechanism of GAPR-1 interaction with membranes. We previously suggested that dimerization plays a role in the function of GAPR-1 and here we report that phytic acid (inositol hexakisphosphate) induces dimerization of GAPR-1 in solution. Elucidation of the crystal structure of GAPR-1 in the presence of phytic acid revealed that the GAPR-1 dimer differs from the previously published GAPR-1 dimer structure. In this structure, one of the monomeric subunits of the crystallographic dimer is rotated by 28.5°. To study the GAPR-1 dimerization properties, we investigated the interaction with liposomes in a light scattering assay and by flow cytometry. In the presence of negatively charged lipids, GAPR-1 caused a rapid and stable tethering of liposomes. [D81K]GAPR-1, a mutant predicted to stabilize the IP6-induced dimer conformation, also caused tethering of liposomes. [A68K]GAPR-1 however, a mutant predicted to stabilize the non-rotated dimer conformation, is capable of binding to liposomes but did not cause liposome tethering. Our combined data suggest that the charge properties of the lipid bilayer can regulate GAPR-1 dynamics as a potential mechanism to modulate GAPR-1 function.

1. Introduction

Golgi-Associated plant Pathogenesis-Related protein 1 (GAPR-1) is a mammalian protein, which is a member of the plant pathogenesis related proteins group 1 (PR-1) superfamily. In plants, PR-1 proteins are upregulated and secreted upon infection and are further characterized by their relatively small molecular mass (14–17 kDa), often acidic or basic nature, and resistance to proteases [1]. Proteins of this family are related to each other based on sequence homology as well as tertiary structure [2,3]. The mammalian PR-1 family member GAPR-1 is highly expressed in immune-related tissues and cells [4]. Therefore, GAPR-1 may play a role in the innate immune system of mammals. The activity and biological function of GAPR-1 and other PR-1 family members remain unknown. Although an anti-fungal activity has been described [5] other publications report a serine protease activity [6]. The highly conserved histidine and glutamate pairs of the PR-1 family have also been proposed to represent a catalytic tetrad, although the arrangement showed no similarities to any previously characterized enzymes [7,8]. We recently suggested that a catalytic triad similar to that of serine proteases may be formed across the dimer interface by residues from both molecules within the dimer [3], implying that dimer dynamics may regulate the activity of the protein.

In contrast to other known PR-1 family members, GAPR-1 is not secreted, but localizes to the cytosolic leaflet of the Golgi membrane [4]. GAPR-1 is strongly bound to Golgi membranes, as salt-stripping of membranes or treatment of cells with Brefeldin A, which causes a redistribution of GAPR-1 in cells, do not release GAPR-1 from membranes [4]. GAPR-1 is myristoylated and fatty acid modification could provide a mechanism to anchor this protein to the membrane. The binding energy of myristate incorporation into lipid bilayers is however not sufficient to stably anchor a protein to a membrane [9]. In support of this, several myristoylated proteins do not show exclusive membrane localization and a second interaction is required for efficient membrane binding (reviewed in [10,11]). GAPR-1 has a pI of 9.4 and therefore GAPR-1 is predicted to have a net positive charge at physiological pH. According to the crystal structure of GAPR-1, several positive charges localize to one protein surface area [3], providing a possibility for efficient

* Corresponding author. Tel.: +31 30 2535375; fax: +31 30 2535492.
E-mail address: j.b.helms@uu.nl (J.B. Helms).
[1] Current address: Centre for Genomic Regulation, c/ Dr. Aiguader, 88, Barcelona, Spain.
[2] These authors contributed equally to this work.
[3] Current address: University of California San Diego, 9500 Gilman Drive, Stein clinical Science, La Jolla, CA, USA.

0005-2736/$ – see front matter © 2012 Elsevier B.V. All rights reserved.
doi:10.1016/j.bbamem.2012.04.016

electrostatic interactions with negatively charged proteins and/or lipids in the membrane. Indeed, we recently described the binding of GAPR-1 to negatively charged lipids *in vitro* [12]. Furthermore, GAPR-1 has been shown to interact with caveolin-1, and interactions with other proteins are possible via a coiled-coil domain [3,4]. Finally, GAPR-1 has been reported to interact with itself, forming homo-dimers [3,4]. Myristoylation, together with protein–protein interactions and/or electrostatic interactions may be sufficient for the stable membrane binding of GAPR-1.

Here we provide evidence for an additional level of regulation of GAPR-1 dynamics at biological membranes. We report that GAPR-1 can adopt a different dimer configuration in the presence of phytic acid (inositol hexakisphosphate). Phytic acid (IP6) has been shown to act as a cofactor of proteins [13–15] or to promote protein oligomerization [16,17]. Our results do not indicate a structural resemblance with these proteins. Rather, we favor the suggestion that the electrostatic interaction of GAPR-1 with phytic acid may resemble an electrostatic interaction of GAPR-1 with other negatively charged structures such as negatively charged lipid bilayers. Hence, the charge properties of lipid bilayers could potentially affect the dimerization dynamics of GAPR-1.

2. Materials and methods

2.1. Reagents

1-palmitoyl-2-oleoyl-*sn*-glycero-3-phosphocholine (POPC), L-a-phosphatidylinositol (bovine liver) and cholesterol were purchased from Avanti Polar Lipids. Phytic acid (inositol hexakisphosphate, IP6) (Cat. no. P8810) and lysozyme from chicken egg white (Cat. no. L6876) were purchased from Sigma (St. Louis, US) and myo-inositol from GIBCO (Grand Island, US). 100 mM IP6 stock solutions were freshly prepared in water and adjusted to neutral pH. Malonate-imidazol boric acid (MIB), malic acid 2-(N-morpholino)ethanesulfonic acid tris(hydroxymethyl)aminomethane (MMT) were purchased from Molecular Dimensions (Suffolk, UK) and poly(ethylene glycol) (PEG) from Sigma (St. Louis, US).

2.2. Plasmids

pQE60-GAPR-1 WT and pQE60-GAPR-1 Δ4 plasmids were described previously [3,18]. [A68K]GAPR-1, [D81K]GAPR-1 and the GAPR-1 lysine mutant were generated by site-directed mutagenesis using polymerase chain reaction (PCR) on the pQE60-GAPR-1 WT plasmid. The following mutagenic primers were used with the changed codons depicted in bold: 5′-gtgtggggagaaccttt**aaa**tgggcatcctatgatc-3′ as the sense primer and 5′-gatcataggatgccca**ttt**aaggttctccccacac-3′ as the antisense primer for the generation of [A68K]GAPR-1; 5′-ggaaaggaggtggct**aag**agatggtacagtgaa-3′ as the sense primer and 5′-ttcactgtaccatct**ctt**agccacctcctttcc-3′ as the antisense primer for the generation of [D81K]GAPR-1. The GAPR-1 lysine mutant was generated in 4 steps: K7S, K53S, K88S and ΔK153-K154. The following mutagenic primers were used: 5′-gggcaagtcagcttccagtcagtttcataatgagg-3′ and 5′-cctcattatgaaactgactggaagctgacttgccc-3′ for K7S, 5′-cacgaggatcctcagtcacagcccggagtc-3′ and 5′-gactccgggctgtgactgaggatcctcgtg-3′ for K53S, 5′-gatggtacagtgaaatcagtaactataacttccagcagcc-3′ and 5′-ggctgctggaagttatagttactgatttcactgtaccatc-3′ for K88S and 5′-cgtcctgccgccgtagaagtaacttgttaaatg-3′ and 5′-catttaacaagttacttctacggcggcaggacg-3′ for ΔK143–K154. Reactions were performed using *Pfu* polymerase (Fermentas, Burlington, Canada). The mutated DNA was selected by restriction-site analysis, transformed into *Escherichia coli* (XL-1 blue, Stratagene, Cedar Creek, US), and subsequently amplified using standard molecular biological techniques. The resulting plasmids were verified by sequencing (Baseclear, Leiden, The Netherlands).

2.3. Protein purification

For the isolation of both wild type and mutant GAPR-1, a shortened protocol was used as described [18]. Briefly, *Escherichia coli* (XL-1 blue, Stratagene) were transformed with the pQE60-GAPR-1 WT, pQE60-[A68K]GAPR-1, pQE60-[D81K]GAPR-1 or GAPR-1 lysine mutant plasmid. While shaking at 300 rpm, bacterial cultures were induced with 1 mM IPTG for 4 h, 37 °C. After incubation the bacteria were pelleted, washed twice in 50-NT buffer (50 mM NaCl, 25 mM Tris pH 7.4), and homogenized by sonication. The homogenate was cleared by centrifugation for 30 minutes at 14,000 rpm and by subsequent passage through a filter with 20 μm pore size. The soluble protein fraction was passed through a cation exchange column using SP Triacryl Plus M. The column was then washed with 50-NT buffer and GAPR-1 (WT or mutant) was eluted from the column with 350 mM NaCl, 25 mM Tris pH 7.4. The purity of the isolated proteins was confirmed by SDS-PAGE and Coomassie Blue staining.

2.4. Crystal structure determination

GAPR-1 was purified as described [3,18]. To crystallize GAPR-1 in the presence of IP6, 11 mg GAPR-1 (1 mg/ml in 10 mM Tris, 50 mM NaCl, pH 7.4) was incubated for 30 minutes at 37 °C in the presence of IP6 (0.7 mM). GAPR-1 was concentrated by use of a spin column (5 kDa cut-off filter) (Vivascience, Hannover, Germany) in a cooled centrifuge to a final concentration of 9.6 mg/ml, corresponding to 0.56 mM. Besides GAPR-1, the protein solution contained 50 mM NaCl, 10 mM Tris pH 7.4 and 0.7 mM IP6. Initial crystallization screening was performed at room temperature by sitting-drop vapor-diffusion. A HoneyBee 961 (Genomic Solutions) crystallization robot was used for pipetting 50 μl of the reservoir solution into the wells and for combining 150 nl protein solution and 150 nl reservoir solution. The initial block-shaped crystals were reproduced and optimized by equilibration of 1 + 1 μl hanging drops. Crystals were obtained at various conditions from either 100 mM MIB-buffer, MMT-buffer or tris(hydroxymethyl)aminomethane-buffer pH 6.5–7.0 and either 15–25% (w/v) PEG 1500, PEG 3350 or PEG 6000. A crystal with dimensions $0.12 \times 0.04 \times 0.03$ mm, that was grown from 100 mM MMT-buffer pH 6.5 and 15% (w/v) PEG 3350, was soaked for 1 minute in a 2-μl cryoprotectant solution containing 22% (w/v) PEG 1500, 100 mM MMT-buffer pH 6.75 and 20% (v/v) glycerol in the presence of 5 mM IP6 and then picked up using a fiber loop prior to flash cooling of the crystal by immersion in liquid nitrogen. A data set was collected at 100 K on a CCD detector (MAR Research) at ID23-2 at the ESRF at a resolution to 1.5 Å. The wavelength used was 0.8726 Å, the total oscillation was 90° with an 0.5° oscillation step per diffraction frame. The crystal belongs to the orthorhombic space group $C222_1$ with unit cell dimensions $a = 44.1$, $b = 64.9$ and $c = 103.1$ Å. Data collection and processing statistics are given in Table 1. The data were integrated with MOSFLM [19] and scaled using SCALA [19]. The structure was determined by molecular replacement with Phaser [20]. The structure of GAPR-1 in the absence of IP6 (Protein Data Bank entry 1SMB) [3] was used as search model. Manual adjustments of the model were carried out with COOT [21] and REFMAC5 [19] was used for subsequent refinements. The solvent content calculated was 41% (v/v) with a V_m value of 2.1 $Å^3$/Da. The electron density for residues 4–152 was clearly interpretable. Residual density at the C-terminus allowed elongation of the polypeptide chain with residues Lys153 and Lys154. However, Lys153 and Lys154 showed poor side-chain density. In addition poor side-chain density was observed for Lys7, Lys33 and Lys88. At the interface of 4 crystallographic symmetry-related GAPR-1 molecules the $F_o - F_c$ difference map indicated an area of positive electron density (≥ 3.5-6σ) that was surrounded by several positively charged residues. The density showed features of IP6, but disorder was apparent. We decided to model IP6 in the density map at half occupancy

Table 1
Data collection and refinement statistics for GAPR-1 with phytic acid.

Data collection	
Space group	$C222_1$
Cell dimensions *a*, *b*, *c* (Å)	44.1, 64.9, 103.1
Resolution (Å)	22–1.5 (1.58–1.5)
R_{merge} (%)	8.5 (43.3)
$I/\sigma I$	9.9 (3.4)
Completeness (%)	91.8 (94.7)
Redundancy	4.0 (3.8)
Unique reflections	21759 (3260)
Mosaicity (°)	0.45
Refinement	
Resolution (Å)	36–1.5 (1.54–1.5)
No. reflections	20632 (1552)
No. free-*R* reflections (5.1%)	1116
R_{work} / R_{free} (%)	15.2 (20.1)/18.7 (25.5)
No. atoms	1434
Residues	1225
Phytic acid	36
Waters	173
Average *B*-factors (Å^2)	10.1
all	7.9
Protein	40.8
Phytic acid	19.4
Water	
R.m.s. deviations	0.022
Bond lengths (Å)	1.83
Bond angles (°)	
Total No. residues	151
Double conformations	Ser43, Ser48, Ser58, Ser71, Met107, Met115, Ser121, Ser127
Restrained refinement weighting factor	2.0
TLS group definitions (residue numbers)	4–32, 33–72, 73–103, 104–154

Values in parentheses refer to the highest resolution shell.

(the model of IP6 was from Protein Data Bank entry 3HO6). Surprisingly, despite co-crystallization of GAPR-1 in excess of IP6 and soaking of crystals in excess IP6 (5 mM; data not shown), the incorporation of IP6 did not improve. In accordance with the structure from Protein Data Bank entry 1SMB, a cysteinesulfonic acid residue at residue 32 was assigned. However, the density for residue 63 unambiguously indicated a cysteine, and not a cysteinesulfonic acid residue as in 1SMB. The final model contained 151 amino acid residues (residues 4–154) corresponding to one monomer of GAPR-1 and 173 water molecules in the asymmetric unit. In total 8 residues have been modeled in two equal populated independent conformations in accordance with the observed electron densities. The final refined model, achieved after several cycles of refinement using REFMAC5 with the application of 4 consecutive TLS groups, had an *R* factor and an R_{free} of 15.2% and 18.7%, respectively. The stereochemistry displayed by the Ramachandran plot shows that 97.7% of the residues fall in the most favored region and 2.3% in the additional allowed region. Statistics on the model quality are given in Table 1. All molecular graphics figures were generated with pymol (W. Delano; http://www.pymol.org/). Coordinates and structure factors have been deposited in the Protein Databank Bank (accession No. 4AIW).

2.5. Liposome binding assay

The liposome binding assay was performed as described [12]. In short: Stock solutions of lipids were made in chloroform:methanol (1:2) and stored at −20 °C under N_2 atmosphere. Liposomes were made freshly for each liposome binding assay. To generate liposomes, phosphatidylcholine, phosphatidylinositol and cholesterol were mixed from stock solutions at a molar ratio of 1.82:0.46:1 or at a ratio as indicated in the figure legend. The solvents were evaporated using a flow of N_2 with subsequent drying at room temperature in a Speedvac (Savant SVC100H Farmingdale, US) for at least 90 minutes. 50-NT buffer was added to the dried lipid film to a final phospholipid concentration of 17 mM. The tube was vortexed at least 3 times for 15 seconds until all lipids had been suspended. To create liposomes, the lipid suspension was sonicated 4 times for 15 seconds on ice using an ultrasonic probe (MSE Soniprep 150, London, UK). The liposomes were relatively uniform in size (90–120 nm) with an average size of 100 nm as determined by nano particle tracking analysis (NanoSight Ltd., Salisbury, United Kingdom).

In a typical experiment, 20 μg recombinant GAPR-1, 100 μg bovine serum albumin (BSA) (Roche, Basel, Switzerland) as carrier protein, 20 μl of the liposome mixture, and the indicated concentrations of IP6 were incubated in 50-NT buffer (90 μl total volume) for 90 minutes at 37 °C. The incubations were stopped by cooling the samples on ice. Sucrose (60% (w/v) in 50-NT) was mixed with the samples to a final concentration of 36.5% (w/v) sucrose. The samples were overlayed with 500 μl 25% (w/v) sucrose in 50-NT buffer and subsequently with 100 μl 50-NT buffer and centrifuged in a TLA-55 rotor (Beckman, Fullerton, US) for 90 minutes at 55,000 rpm, 4 °C. After centrifugation, protein bound to liposomes was collected in 300 μl from the top of the gradient.

2.6. Gel filtration

Dimerization of GAPR-1 or GAPR-1:IP6 complexes was determined by gel filtration. Briefly, a 30/10 Pharmacia column containing Superdex 200 (Pharmacia, Uppsala, Sweden) was equilibrated with 50-NT buffer (50 mM NaCl, 25 mM Tris pH 7.4). To estimate the size of the GAPR-1-complexes, myoglobulin (18 kDa), ovalbumin (45 kDa), bovine serum albumin (67 kDa) and bacitracin (1.4 kDa) were used as reference proteins (ICN Biomedicals, Aurora, US). GAPR-1 was incubated in 50-NT buffer with or without 1 mM IP6 in 100 μl total volume for 30 minutes at 37 °C. The protein solution was then cooled to 4 °C, after which it was loaded on the column and eluted at 0.5 ml/min at 4 °C. The eluent was collected in fractions of 0.5 ml. The protein content of the fractions was determined by absorbance at 280 nm. Elution of GAPR-1 was determined by Western blotting using a polyclonal GAPR-1 antibody [4]. Elution of IP6 was measured by phosphate determination using a modified spectrophotometric protocol according to Rouser [22]. Briefly, 400 μl of each fraction was taken and water was evaporated by heating. The residue was resuspended in 150 μl 70% perchloric acid and heated to 180 °C for 1 h. Samples were cooled and then incubated with 625 μl H_2O, 125 μl 2.5% ammoniumheptamolybdate and 125 μl 10% (w/v) ascorbic acid at 55 °C for 20 minutes. Absorbance of the samples was measured at 820 nm wavelength and compared with that of standard solutions of IP6.

2.7. Gel electrophoresis

Proteins were resolved on 14% polyacrylamide gels. Gels were analyzed by staining with Coomassie Blue R250 (Serva Electrophoresis, Heidelberg, Germany) or by Western blotting. In the case of Coomassie Blue staining, protein amounts were determined by optical scanning of the Coomassie Blue-stained bands and analysis by use of Quantity One software (Biorad, Hercules, US). The binding of GAPR-1 to liposomes in the absence of IP6 was used as a reference (100%). For Western blotting, an affinity-purified polyclonal rabbit antibody against GAPR-1 was used as described [4]. Peroxidase-labeled goat anti-rabbit (Nordic Immunology, Tilburg, The Netherlands) was used as secondary antibody. Supersignal West Pico Chemiluminescent was purchased from Pierce (Rockford, US). Chemiluminescence was captured with a Chemidox XRS camera (Biorad) and signals were quantified using Quantity One software package (Biorad). Signals from the incubations were compared to standard curves with known amounts of GAPR-1.

2.8. Light scattering assay

The turbidimetric method was originally developed by Bangham et al. to determine the osmotic behavior of the multilamellar liposomes [23]. This principle also allows analysis of clustering of liposomes [24]. The turbidity of the liposome suspension was measured at a wavelength of 600 nm using an Eppendorf Biophotometer and a 10 mm path length UVette® (Eppendorf, Hamburg, Germany). A typical reaction mixture consisted of 10 µl GAPR-1, 20 µl liposome mixture (prepared as described earlier) in 50-NT buffer in a final volume of 90 µl. First, the OD of the liposome suspension was measured, after which the protein was added. After brief mixing the OD was monitored in time.

2.9. Flow cytometric analysis

For flow cytometry, liposomes were prepared as described above, except that lipid films were hydrated in the presence of 3 mM calcein in 50-NT. Following sonication, non-encapsulated calcein was removed by size-exclusion chromatography (Sephadex G-50, fine) using 50-NT as elution buffer.

To analyze the ~100 nm sized fluorescently-labeled liposomes, we used a recently developed flow cytometry-based method for multiparameter analysis of individual nano-sized particles [25]. For these measurements, the BD Influx™ flow cytometer (Becton Dickinson) was triggered on the fluorescence signal derived from the fluorescently labeled liposomes and thresholding was applied on this fluorescence channel. Fluorescence thresholding was based on measuring 0.22 µm filtered PBS, allowing an event rate of not more than 6 events per second. Light scattering detection was performed in log mode. Samples were measured at event rates lower than 10,000 events per second. Typical reaction mixtures were appropriately diluted in 50-NT buffer immediately before flow cytometric analysis.

3. Results

3.1. Phytic acid inhibits binding of GAPR-1 to phosphatidylinositol

To investigate the contribution of lipids to GAPR-1 membrane binding, a liposome binding assay was performed which showed that GAPR-1 binds to phosphatidylinositol (PI) but not to phosphatidylcholine (PC) [12]. A systematic screen of potential effectors of the GAPR-1 liposome binding assay was performed. After incubation, the liposome-bound GAPR-1 was floated on a sucrose gradient and liposome-bound proteins in the top fraction were quantified. When GAPR-1 was incubated with PI-containing liposomes for 90 minutes at 37 °C, approximately 20% of GAPR-1 bound to liposomes (Fig. 1A). This is in agreement with previous observations [12]. When GAPR-1 was incubated with the liposomes in presence of *myo*-inositol or *meso*-inositol, the binding of GAPR-1 to the liposomes was not affected. However, when the incubation was performed in presence of phytic acid (IP6, inositol hexakisphosphate), the binding to liposomes was strongly reduced (Fig. 1A). Quantification of GAPR-1 binding efficiency at various concentrations of IP6 showed half maximal inhibition of GAPR-1 binding at 50–60 µM IP6 (Fig. 1B).

3.2. Phytic acid induces dimerization of GAPR-1

IP6 is known to promote oligomerization of arrestin-2 and trimerization of the HIV Gag protein [16,17]. Interestingly, dimerization has been implicated in the function of GAPR-1 [3]. Therefore, we investigated whether GAPR-1 also dimerizes or oligomerizes in the presence of IP6. To test this, GAPR-1 was incubated in the absence or presence of IP6 and the size of the GAPR-1 complex was estimated by gel filtration chromatography. In the absence of IP6, GAPR-1 eluted from the column as a protein with an apparent molecular mass of 10 kDa (Fig. 1C). When incubated with IP6, GAPR-1 migrated faster on the column, with an apparent molecular mass of 20 kDa. This indicates that IP6 promotes dimerization of GAPR-1. To exclude a formal possibility that the shift from 10 kDa to 20 kDa is caused by non-specific electrostatic binding of a large number (15 molecules of IP6

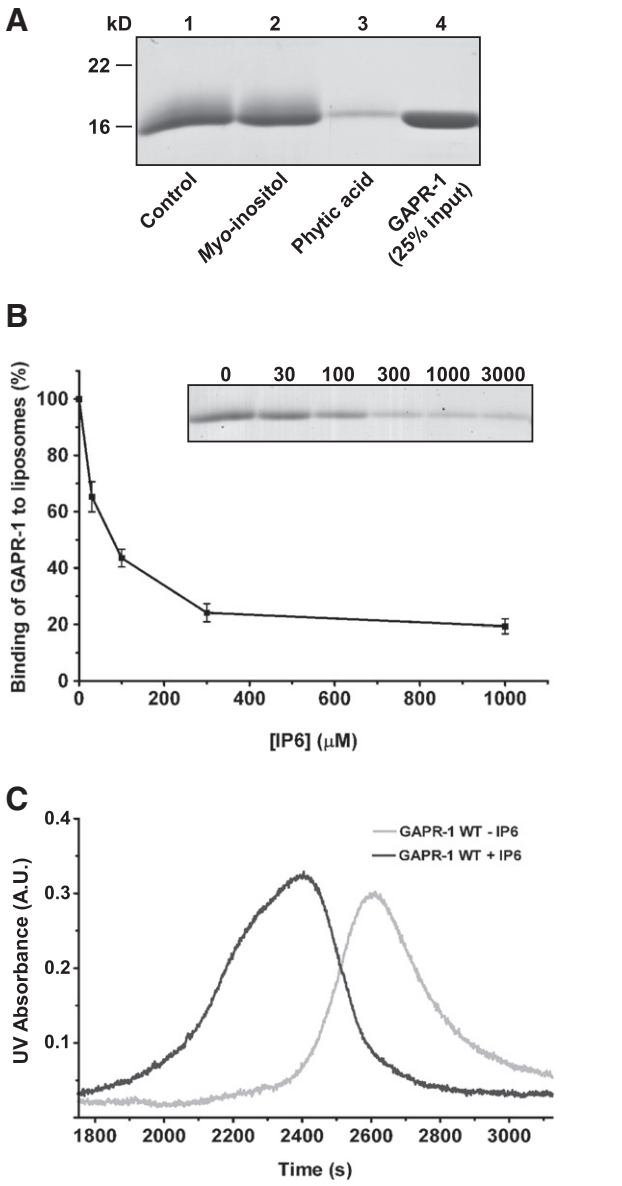

Fig. 1. Membrane binding of GAPR-1 is inhibited by phytic acid. A. Competition assay for GAPR-1 binding to PI-containing liposomes. To generate liposomes, phosphatidylcholine, phosphatidylinositol and cholesterol were mixed from stock solutions at a molar ratio of 1.94:0.34:1. GAPR-1 (lane 4, ¼ of input) was incubated with liposomes (containing PI, POPC and cholesterol), bovine serum albumin (BSA) (carrier protein) and buffer in the absence (lane 1) or presence of 5 mM inositol (lane 2) or 5 mM IP6 (lane 3) for 90 minutes at 37 °C. After flotation on a sucrose gradient, proteins bound to liposomes were resolved by SDS-PAGE and stained with Coomassie Blue. B. Titration of IP6. IP6 was titrated (0–3000 µM) in the liposome binding as described for (A). Proteins bound to liposomes were resolved by SDS-PAGE and stained with Coomassie Blue. The insert shows a typical experiment over the entire range of titration. To determine half-maximal inhibition, the intensity of the Coomassie Blue-stained bands were quantified by optical scanning and plotted as binding percentage relative to the binding in the absence of IP6. Bars represent the standard deviation. C. Gel-filtration chromatography of GAPR-1 WT in the absence and presence of IP6. GAPR-1 (40 µg) was incubated in buffer in the absence (gray line) or presence (black line) of 1 mM IP6 for 30 minutes at 37 °C. The samples were resolved by gel-filtration chromatography and eluted proteins were detected by UV absorption. To calibrate the column, ovalbumin, BSA, myoglobin, chymotrypsin, and bacitracin were used as reference proteins.

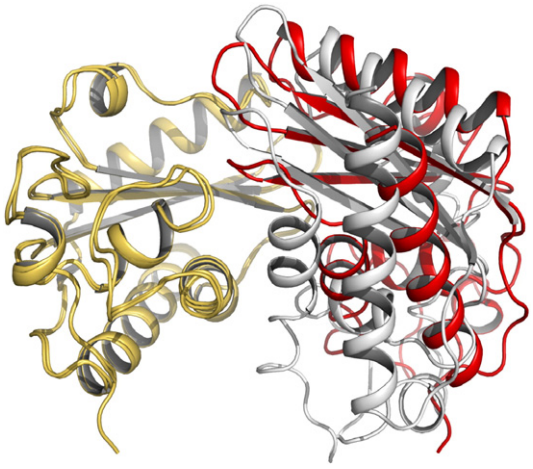

Fig. 2. Superposition of GAPR-1 dimer structures in the absence and presence of IP6. The monomeric structures are superimposed using residues 4–152. The left monomers (yellow) are positioned in the same orientation to allow visualization of the rotation of the partner monomers at the right (partner monomer of the open dimer structure in the presence of IP6 in red). For structural visualization of the GAPR-1 dimer in the absence of IP6, Protein Data Bank entry 1SMB was used.

correspond to about 10 kDa) of IP6 molecules to GAPR-1, the stoichiometry of the IP6-GAPR-1 interaction was determined by measuring the phosphate and protein content in the eluted fractions of the gel-filtration experiments. In the peak fraction approximately a 1:1 ratio of protein:IP6 was found, demonstrating that the shift of IP6-bound GAPR-1 is not caused by binding multiple IP6 molecules to GAPR-1.

3.3. The crystal structure of the GAPR-1 dimer in the presence of phytic acid shows rotation of GAPR-1 monomers

We performed X-ray crystallography to determine the effect of IP6 on the GAPR-1 dimer structure. Comparing the structures of the monomeric subunits in the absence and presence of IP6 resulted in a r.m.s. fit for 149 aligned Cα positions of 0.47 Å, indicating a good structural agreement between GAPR-1 monomers in the absence or presence of IP6 (Suppl. Fig. 1). In the presence of IP6, one of the monomeric subunits of the crystallographic dimer is rotated by 28.5°, relative to the previously reported GAPR-1 dimer structure, which was determined in the absence of IP6 [3] (Fig. 2). As a consequence of the rearrangement the interface between the GAPR-1 monomers has become smaller, resulting in a more open dimeric structure (Fig. 3). Hereafter we will refer to the rotated dimer structure in the presence of IP6 as 'open dimer', and the dimer structure in the absence of IP6 as 'closed dimer'. In the closed dimer structure, the interface area of the dimer calculated by PISA [26] was 943 Å^2 (11.7%) and for the open dimer structure in presence of IP6 717 Å^2 (8.6%).

A significant difference between both dimer interfaces is a predominant hydrophilic patch formed by residues 77–89 in the closed dimer interface that is lacking in the open dimer interface (Fig. 3). There is also a major change in orientation of the side chain of residue Lys88, resulting in an entire opening of the cleft in the open dimer. The closed dimer has a single salt bridge between Lys88 and Asp81 of the partner monomer, whereas the open dimer has a salt bridge between Arg50 and Leu52 across the dimer interface.

Due to reorientation of the monomers, the putative catalytic triad, consisting of His54, Glu65 and a symmetry-related Ser71 [3], formed across the dimer interface by residues from both molecules within the dimer, is disrupted. The distance between His54 $N^{\varepsilon 2}$ and Ser71 O^{γ} of the partner monomer is significantly changed from 4.2 Å to 5.7 Å in the presence of IP6; with all intramolecular distances of the putative catalytic residues being the same.

The position of IP6 in the open structure could not be unambiguously determined. It was possible, however, to model IP6 in the F_o-F_c difference map. An additional buried-surface area of 269 Å^2 was calculated with PISA for IP6 in which IP6 is surrounded by several positively charged residues belonging to different GAPR-1 molecules. In this model, residues that make a putative salt bridge with IP6 are Lys7 and Lys33 (molecule 1), Lys53 (molecule 2), Lys88 and Lys154 (molecule 3), and Arg50 (molecule 4). Of these residues Lys33 and Lys88 are further away from IP6, but could possibly contribute additionally to the ligand binding site (Suppl. Fig. 2). However, mutation of Lys7, Lys53 and Lys88 to serine and deletion of Lys153 and Lys154 using site directed mutagenesis did not affect the inhibition of GAPR-1 membrane-binding by IP6 and IP6 still caused dimerization (Suppl. Fig. 3). This suggests that the modeling

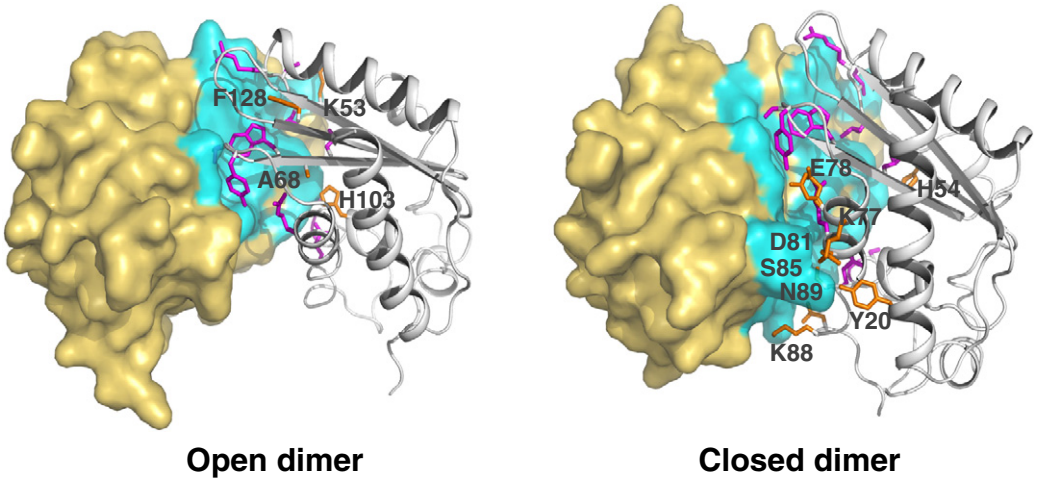

Fig. 3. Interface of the open and closed GAPR-1 dimer configurations. Dimers in the presence (left panel) or absence (right panel) of IP6, showing the relative rotation of the subunits of the dimers. IP6 is omitted from the figure in the left panel. The monomers of the crystallographic dimers are packed face-to-face. At the interfacial region the molecular surface representation is shown in cyan and the involved residues of the dimeric partner molecule are indicated as sticks. Common dimer-interface residues (Arg50, Ile51, Leu52, Leu67, Trp69, Ser71, Tyr72, Arg82, Glu86, Ser99 and Gly100) are colored magenta and are unlabeled, the other additional residues (closed dimer-interface additional residues are Tyr20, His54, Lys77, Glu78, Asp81, Ser85, Lys88 and Asn89; open dimer-interface additional residues are Lys53, Ala68, His103 and Phe128) are colored orange and labeled accordingly. In both panels, the left monomer (yellow) is positioned in the same orientation to allow visualization of the rotation of the partner monomer (right monomer in both panels). Residues within contact distance of 4 Å observed at the dimer interface in both structures are shown. Of note, in the presence of IP6, residues Lys153 and Lys154 could be assigned, resulting in a small extended structure (left panel, near the bottom of the left (yellow) monomer).

of IP6 in the crystal structure needs further improvement. The modeling of IP6 was based on the identification of an area with positive electron density (≥ 3.5-6σ) with features of IP6, but disorder was apparent (see Materials and methods). Thus, although we do not doubt the location of IP6 in the crystal structure, alternative IP6 orientations may be possible.

3.4. Inhibition of membrane binding is not dependent on dimer configuration

To investigate the potential significance of the IP6-induced rotation in the dimer, GAPR-1 mutants were designed to stabilize different dimer configurations. Alanine 68 (A68) is involved in stabilization of the open (rotated) dimer (Fig. 3). When A68 is replaced by lysine, rotation of GAPR-1 monomers relative to each other in the dimer will not be favorable, as the lysine is in close proximity of a tryptophan residue (W69) of the other monomer. By contrast, aspartic acid 81 (D81) is a prominent amino acid involved in the stabilization of the closed conformation by interaction with lysine 88 (Fig. 3) in the opposite facing monomer. When D81 is replaced by lysine, ionic repulsion may destabilize the closed conformation. To test whether [A68K]GAPR-1 and [D81K]GAPR-1 mutants are still able to interact with IP6, the behavior of these mutants were analyzed by gel filtration chromatography (Fig. 4A). When [A68K]GAPR-1 was incubated with IP6, a shift in apparent molecular mass was observed that closely resembled the shift described above for wild type GAPR-1 in the presence of IP6 (Fig. 1C), indicating that [A68K]GAPR-1 mutant is able to interact with IP6. Similar results were obtained for [D81K]GAPR-1 (data not shown). As GAPR-1 wild type forms the open dimer conformation in the presence of IP6, this may indicate that the open dimer conformation is favorable in the presence of IP6 under normal circumstances.

To investigate whether the IP6-induced rotation is the cause of the observed inhibition of membrane binding of GAPR-1, a liposome binding experiment was performed with the [A68K]GAPR-1 and [D81K]GAPR-1 mutants in presence or absence of IP6. As shown in Fig. 4B, both mutants bind efficiently to liposomes and the binding of both mutants is inhibited by IP6. Thus, inhibition of membrane binding is not dependent on a particular dimer configuration.

3.5. GAPR-1 membrane-binding causes dimerization

Our observations raise the question how IP6 inhibits membrane binding of GAPR-1 to negatively charged liposomes. The first possibility is that dimerization per se inhibits membrane binding. This seems unlikely as GAPR-1 dimers have been identified on isolated Golgi membranes [4]. The second possibility is that IP6 resembles some properties (charge and/or structure) of the lipid bilayer and competes with membranes for interaction with GAPR-1. A consequence of the IP6-mimicking properties of membranes is that it would predict dimerization of GAPR-1 upon membrane-binding. To investigate this, we employed an assay that measures clustering of liposomes by light scattering [23,24]. Liposome-bound GAPR-1 may bring together liposomes upon dimerization, resulting in increased particle sizes, which in turn causes increased light scatter and absorbance. Liposomes of different composition were incubated with GAPR-1 WT or mutant proteins at room temperature and the clustering of liposomes was determined by measuring the absorbance of the incubation at 600 nm. As shown in Fig. 5A, addition of GAPR-1 wild type to liposomes results in a rapid increase in light scattering. The increased absorbance remains stable for at least 60 minutes, indicating that a steady state level has been reached. Similar results were obtained with [D81K]GAPR-1 mutant, but

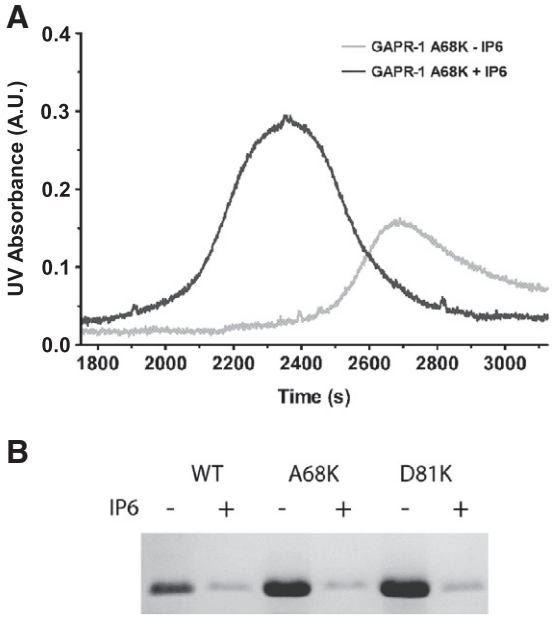

Fig. 4. Phytic acid induces dimer formation and inhibits membrane binding of [A68K]GAPR-1 and [D81K]GAPR-1. A. Gel-filtration chromatography of [A68K]GAPR-1 (40 μg) in the absence (gray line) and presence (black line) of 1 mM IP6. B. Competition assay for GAPR-1 binding to PI liposomes. GAPR-1 WT, [A68K]GAPR-1 and [D81K]GAPR-1 were incubated with liposomes in the absence or presence of 1 mM IP6 for 90 minutes at 37 °C. GAPR-1 binding to liposomes was analyzed by SDS-PAGE (upper panel). Shown is a representative experiment ($n = 3$).

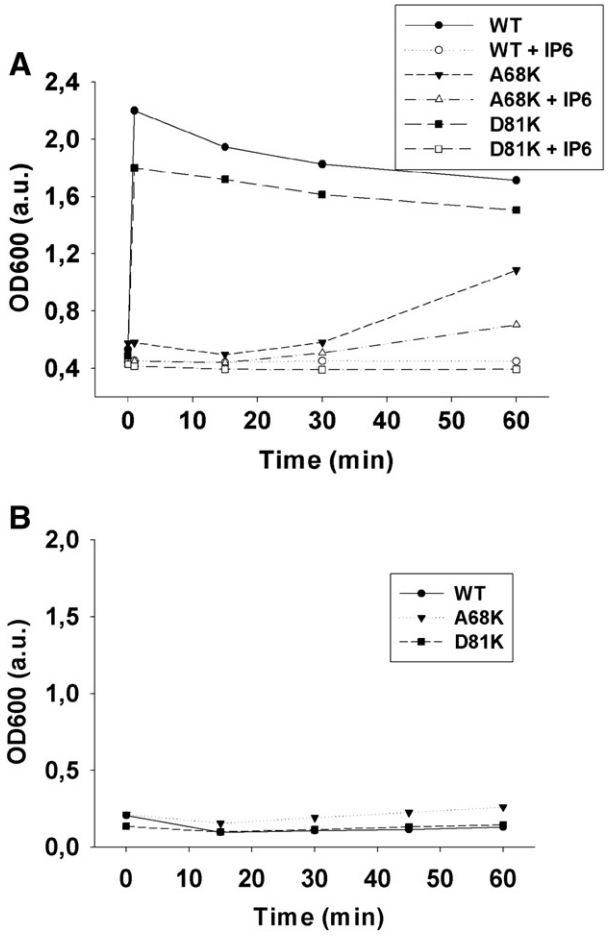

Fig. 5. WT GAPR-1 causes liposome clustering, which is dependent on the dimer conformation. Light scattering assay. Optical density ($\lambda = 600$ nm) of liposome suspension is monitored in time, following the addition of GAPR-1 WT, [A68K]GAPR-1 and [D81K]GAPR-1, respectively. Panel A: At $t = 0$, protein was added to a suspension of PC/PI/cholesterol liposomes (molar ratio 1.82:0.46:1) in 50-NT buffer, in the absence or presence of IP6 (1 mM); Panel B: At $t = 0$, protein was added to a suspension of PC/cholesterol liposomes (molar ratio 2.28:1) in 50-NT buffer.

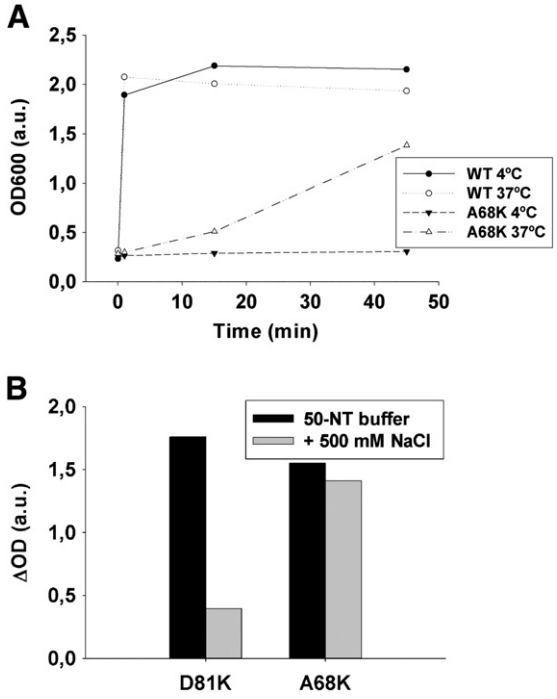

Fig. 6. WT and [D81K]GAPR-1 clustering of liposomes is driven by electrostatic interactions. A. Temperature dependence of light scattering changes upon addition of GAPR-1 to liposomes. Optical density (λ = 600 nm) of liposome suspension is monitored during incubation with GAPR-1 WT or [A68K]GAPR-1 at either 4 °C or 37 °C. A representative chart is shown ($n = 3$). B. Sensitivity of increased light scattering towards high salt concentration. PC/PI/cholesterol liposomes were incubated with [A68K] or [D81K]GAPR-1 for 60 minutes at 37 °C and the increase in light scattering as compared to liposomes in the absence of protein (ΔOD) was determined (black bars). NaCl was then added to a final concentration of 500 mM (grey bars). A representative chart is shown ($n = 3$).

surprisingly, [A68K]GAPR-1 mutant showed different kinetics as it did not result in an increase in light scattering for 20 minutes, with a subsequent slow but steady increase of light scattering. The question arises whether this is caused by a difference in dimer conformation on the membrane or perhaps merely by slower binding kinetics of the A68K mutant. The overall binding kinetics of [A68K]GAPR-1 mutant were, however, shown to be identical to that of GAPR-1 WT (Fig. 4B and data not shown). This rules out the possibility that the absence of a rapid increase in light scattering for [A68K]GAPR-1 is due to a lack of binding. Therefore, these results show that the assay is capable of measuring differences in light scattering between different GAPR-1 mutants representing the open and closed dimer configuration.

In agreement with our hypothesis that IP6 mimics some properties of membranes, we found that addition of IP6 also effectively inhibits the increase of particle size in the light scattering assay (Fig. 5A). We obtained similar results with phosphatidic acid-containing liposomes (data not shown). This suggests that the interaction of GAPR-1 with negatively charged PI liposomes is based on electrostatic forces that are effectively disrupted by IP6. In the absence of negatively charged lipids, GAPR-1 does not induce light scattering (Fig. 5B).

The aberrant kinetics of [A68K]GAPR-1 mutant were further investigated by incubation at 4 °C and 37 °C. As shown in Fig. 6A, the slow and steady increase of light scattering caused by [A68K]GAPR-1 mutant is temperature dependent. No increase in scattering is observed after prolonged incubation at 4 °C, whereas the kinetics of tethering induced by GAPR-1 wild type is temperature independent. This may suggest that the observed increase in light scattering caused by [A68K]GAPR-1 mutant is not solely based on ionic interactions. In agreement with this suggestion, we found that the increased light scattering caused by prolonged incubation with [A68K]GAPR-1 is insensitive to high salt concentrations, whereas for [D81K]GAPR-1 and wild-type the increase in optical density is reversible at any time point by the addition of 500 mM NaCl (Fig. 6B). Further support comes from the observation that IP6 is a less effective inhibitor of this A68K mutant in the light scattering assay (Fig. 5A).

3.6. GAPR-1 induces tethering of liposomes

The interaction of GAPR-1 with liposomes was further analyzed by a high resolution flow cytometry-based method, which was recently developed to characterize individual particles with sizes that fall below the detection limit of conventional flow cytometers (300 nm) [25]. The ~100 nm sized liposomes could be observed above the fluorescence threshold (Fig. 7). In the absence of GAPR-1, calcein-loaded liposomes appeared as a relatively homogeneous population based on forward light scatter (FSC) and calcein signals. Addition of GAPR-1 caused a shift in light scatter (FSC) as well as in fluorescence of a distinct subset of events (Fig. 7). The concomitant increase of fluorescence with particle size has several implications as i) it rules out the possibility that GAPR-1 forms large aggregates on a single liposome causing an increase in scattering but not fluorescence; and ii) the liposomes with increased scatter remain sealed and do not release their soluble luminal fluorescent dye which would cause a non-linear increase in fluorescence with increasing scatter. The GAPR-1 induced clustering of liposomes is fully reversible as subsequent treatment with IP6 restored the fluorescent characteristics resembling the original liposome population (Fig. 7). This demonstrates that GAPR-1 induced clustering of liposomes reflects a tethering rather than a fusion process.

GAPR-1 dimerization between liposomes is expected to compete with GAPR-1 dimerization on individual liposomes. This may explain the fact that only a subset of liposomes clusters and GAPR-1 is not capable of clustering all liposomes. To test this further, we determined the dependency of tethering on GAPR-1 concentration. At high concentrations of GAPR-1, more GAPR-1 is expected to bind to liposomes [12]

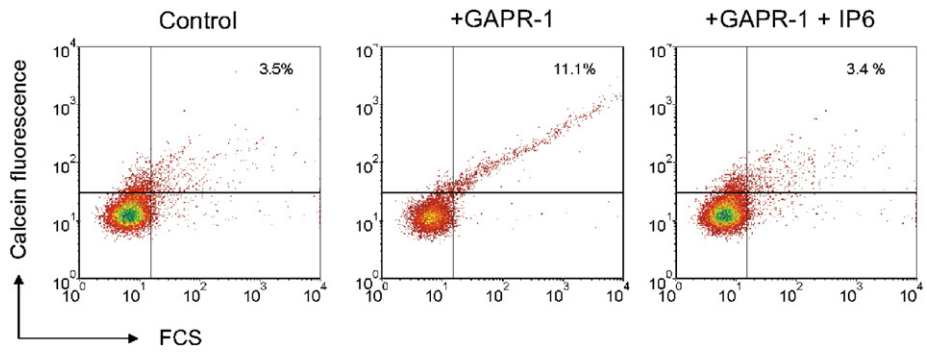

Fig. 7. GAPR-1 induces tethering of liposomes. Liposomes fluorescently labeled with calcein were visualized by high-resolution flow cytometric analysis using a threshold on calcein fluorescence. Shown are dot plots of FSC versus calcein fluorescence representing control liposomes (left), liposomes incubated with GAPR-1 (middle) and liposomes incubated with GAPR-1 and IP6 (right). Numbers indicate the percentage of events in the upper right quadrant, representing clustered liposomes.

increasing the possibility of forming dimers on individual liposomes and reducing the formation of dimers between liposomes. Indeed, with increasing concentrations of GAPR-1 the tethering decreased again. As a control we incubated the same liposomes with lysozyme, which is similar in size and charge to GAPR-1 and known to cause aggregation and fusion of liposomes [27]. In contrast to GAPR-1, lysozyme induced a concentration-dependent but continuously increasing signal in light scattering with increasing concentrations of lysozyme (Fig. 8).

4. Discussion

4.1. GAPR-1 dimerization

GAPR-1 has a tendency to form homo-dimers. A minority (9%) of soluble recombinant non-myristoylated GAPR-1 is dimerized *in vitro*. Crosslinking experiments showed that GAPR-1 forms homo-dimers on membranes [3]. In addition, GAPR-1 crystallizes as a dimer [3]. GAPR-1 *in vivo* can also form homo-dimers, as GAPR-1 interacts with itself in a yeast 2-hybrid system [3]. We now report that GAPR-1 dimerizes in the presence of IP6. Oligomerization by IP6 has been observed for other proteins as well. The HIV-1 protein Gag is in a monomer-dimer equilibrium and in the presence of IP6 this equilibrium shifts towards monomer–trimer [16]. Another example of a protein that is oligomerized by IP6 is arrestin-2, a regulator of G-coupled receptors [17]. In the case of arrestin-2, a high and low affinity binding site for IP6 was identified in the crystal structure. Binding of IP6 to arrestin-2 did not cause a significant global conformational change or rearrangement [17]. Crystal structure analysis of individual GAPR-1 monomers also did not show any major conformational change in the presence of IP6. The 3D model of IP6-treated GAPR-1 shows however that one of the monomeric subunits of the GAPR-1 dimer is rotated by 28.5° in the dimer configuration, relative to the previously reported dimer configuration.

To determine the effect of this rotation on the GAPR-1 binding properties, we generated an [A68K]GAPR-1 mutant in which the rotation of the dimer is destabilized to favor the closed conformation, and a [D81K] GAPR-1 mutant which favors the open dimer conformation. By light scattering we were able to demonstrate that only the open conformation supports tethering of lipid bilayers.

4.2. GAPR-1 and phytic acid

In cells, IP6 has been reported as a cofactor for the yeast RNA editing enzyme ADAR2, for the plant Fbox protein TIR1 and for the mammalian autocatalytic cleavage of Toxin B from *Clostridium difficile* [13–15]. It is possible that IP6 is a cofactor for GAPR-1 as well. Dimerization of GAPR-1 results in the formation of a putative catalytic triad [3]. Rotation of the dimer by IP6 may disrupt the catalytic triad, negatively regulating e.g. the putative serine protease activity of GAPR-1. IP6 competes for membrane binding of GAPR-1 in the micromolar range. This is within the range of physiological IP6 concentrations of mammalian cells (10–100 μM) [28–30]. Therefore, variations of cytosolic IP6 concentrations may have a direct effect on GAPR-1 dynamics and function.

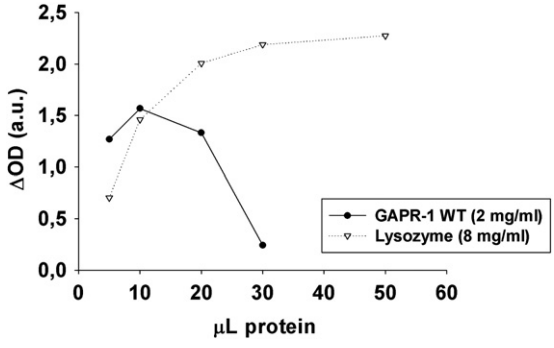

Fig. 8. Tethering of liposomes is dependent on the ratio of GAPR-1 and negatively charged lipids in liposomes. Changes in optical density of liposome suspensions by the addition of increasing amounts of GAPR-1 WT and lysozyme, respectively. Protein was added in the indicated amounts to a PC/PI/cholesterol (1.82:0.46:1) liposome suspension in 50-NT buffer (final phospholipid concentration 3,78 mM). Each measurement was performed 1 minute after adding the protein and it was verified that the OD remained subsequently stable.

By gel filtration we show that treatment of GAPR-1 with IP6 results in the formation of a stable dimer of GAPR-1. The orientation of IP6 in the open structure could, however, not be unambiguously determined. Attempts to co-crystallize GAPR-1 in excess of IP6 and soaking of crystals in excess IP6 did not improve the electron density for IP6. An area of positive electron density was observed at the interface of 4 symmetry-related GAPR-1 molecules that was surrounded by several positively charged residues. The density showed features of IP6, but disorder was apparent. IP6 was modeled in the density map and included in the refinement. The putative GAPR-1 binding site for IP6 was compared with other known IP6-interacting proteins. Currently, the PDB contains 34 files with IP6 (defined as IHP). TIR1 domains bind IP6 with the surrounding basic residues mainly oriented towards the equatorial phosphate groups [15]. This domain lacks structural resemblance with GAPR-1. Non-TIR1 PDB files show diverse manners of IP6 binding. A common feature for all of these sites is a large number (ranging from 5 to 10) of arginines, lysines and sometimes histidines surrounding IP6. A similar surrounding was suggested for the IP6 binding pocket in GAPR-1. However, simultaneous mutation of 5 positively charged amino acids at the proposed interface with IP6 did not affect inhibition of membrane-binding by IP6 and IP6 still caused dimerization.

We consider it likely that the interaction of GAPR-1 with IP6 mimics an electrostatic interaction with other negatively charged structures, possibly negatively charged lipid bilayers. This would explain the competition of IP6 with negatively charged bilayers in the binding assay. Other negatively charged biomolecules such as 2,3 bisphosphoglycerate or inorganic phosphate were, however, much less effective inhibitors of GAPR-1 binding to negatively charged liposomes. These compounds did not affect the GAPR-1 binding assay up to 50-mM. Thus, some structural features of IP6 such as negative charge-density play a role in the inhibitory effect.

4.3. GAPR-1 dynamics and implications

We favor a model in which GAPR-1 monomers are in a dynamic equilibrium with GAPR-1 dimers. This has already been demonstrated for GAPR-1 in solution. Isolation of the dimeric GAPR-1 results in reappearance of monomeric GAPR-1 [3]. Our results now suggest that upon binding to negative charges, GAPR-1 shifts the equilibrium to a particular dimer configuration. Depending on the charge-density, the monomeric subunits of the dimer may be induced to rotate and form an alternative dimeric structure with distinct membrane-binding and tethering properties. It remains to be established whether there is an equilibrium between the open and closed GAPR-1 dimer configuration, but it is tempting to speculate that regulation of the negative charge of a membrane dictates the equilibrium between the open and closed dimer configuration. The binding properties of the closed dimer ([A68K] GAPR-1) are different from the open dimer ([D81K]GAPR-1) configuration. The interaction of [A68K]GAPR-1 mutant with liposomes is temperature dependent and slow as compared to [D81K]GAPR-1 mutant. This indicates that the interaction of [A68K]GAPR-1 mutant with negatively charged lipid bilayers is not entirely electrostatic. Hydrophobic interactions may also be involved in the interaction of [A68K]GAPR-1 mutant with membranes, e.g. by partial insertion into the lipid bilayer. This has been suggested for other myristoylated proteins such as ARF and MARCKS proteins [31].

Thus, dynamics of GAPR-1 dimerization is a novel membrane-binding and conformation determinant that may act synergistically with other known membrane binding determinants such as myristoylation and

protein–protein interactions [3,4]. We have shown that electrostatic interactions with lipid membranes are in principle sufficient to affect GAPR-1 dynamics. This offers potential application to other family members. GAPR-1 belongs to the superfamily of PR-1 proteins and all other family members are secreted as non- myristoylated proteins. In the extracellular space, PR-1 proteins are suggested to interact with the plasma membrane and with pathogens [1]. Both these surfaces are highly negatively charged allowing optimal interaction with the basic members of the PR-1 superfamily. Future investigations will indicate whether these interactions are involved in the regulation PR-1 protein dynamics.

Supplementary materials related to this article can be found online at http://dx.doi.org/10.1016/j.bbamem.2012.04.016.

Abbreviations

GAPR-1	Golgi-Associated plant Pathogenesis-Related protein 1
PI	Phosphatidylinositol
PC	Phosphatidylcholine
POPC	1-palmitoyl-2-oleoyl-*sn*-glycero-3-phosphocholine
IP6	Inositol hexakisphosphate, phytic acid
BSA	Bovine serum albumine
50-NT	50 mM NaCl, 25 mM Tris pH 7.4
FSC	Forward light scatter
MIB	Malonate-imidazol boric acid (MIB),
MMT	Malic acid 2-(N-morpholino)ethanesulfonic acid tris(hydroxymethyl)aminomethane
PEG	Poly(ethylene glycol)

Acknowledgments

We thank Chris van de Lest for help with the FPLC and Coos Batenburg and Bert Janssen for critically reviewing our manuscript. This work was supported by a grant from the Research Council for Earth and Life Sciences (ALW) with financial aid from the Netherlands Organization for Scientific Research (NWO).

References

[1] L.C. van Loon, E.A. van Strien, The families of plant pathogenesis-related proteins, their activities, and comparative analysis of PR-1 type proteins, Physiol. Mol. Plant Pathol. 55 (1999) 85–97.
[2] L.C. van Loon, M. Rep, C.M. Pieterse, Significance of inducible defense-related proteins in infected plants, Annu. Rev. Phytopathol. 44 (2006) 135–162.
[3] R.L. Serrano, A. Kuhn, A. Hendricks, J.B. Helms, I. Sinning, M.R. Groves, Structural analysis of the human Golgi-associated plant pathogenesis related protein GAPR-1 implicates dimerization as a regulatory mechanism, J. Mol. Biol. 339 (2004) 173–183.
[4] H.B. Eberle, R.L. Serrano, J. Fullekrug, A. Schlosser, W.D. Lehmann, F. Lottspeich, D. Kaloyanova, F.T. Wieland, J.B. Helms, Identification and characterization of a novel human plant pathogenesis-related protein that localizes to lipid-enriched microdomains in the Golgi complex, J. Cell Sci. 115 (2002) 827–838.
[5] T. Niderman, I. Genetet, T. Bruyere, R. Gees, A. Stintzi, M. Legrand, B. Fritig, E. Mosinger, Pathogenesis-related PR-1 proteins are antifungal. Isolation and characterization of three 14-kilodalton proteins of tomato and of a basic PR-1 of tobacco with inhibitory activity against Phytophthora infestans, Plant Physiol. 108 (1995) 17–27.
[6] T.J. Milne, G. Abbenante, J.D. Tyndall, J. Halliday, R.J. Lewis, Isolation and characterization of a cone snail protease with homology to CRISP proteins of the pathogenesis-related protein superfamily, J. Biol. Chem. 278 (2003) 31105–31110.
[7] C. Fernandez, T. Szyperski, T. Bruyere, P. Ramage, E. Mosinger, K. Wuthrich, NMR solution structure of the pathogenesis-related protein P14a, J. Mol. Biol. 266 (1997) 576–593.
[8] A. Henriksen, T.P. King, O. Mirza, R.I. Monsalve, K. Meno, H. Ipsen, J.N. Larsen, M. Gajhede, M.D. Spangfort, Major venom allergen of yellow jackets, Ves v 5: structural characterization of a pathogenesis-related protein superfamily, Proteins 45 (2001) 438–448.
[9] R.M. Peitzsch, S. McLaughlin, Binding of acylated peptides and fatty acids to phospholipid vesicles: pertinence to myristoylated proteins, Biochemistry 32 (1993) 10436–10443.
[10] H. Taniguchi, Protein myristoylation in protein–lipid and protein–protein interactions, Biophys. Chem. 82 (1999) 129–137.
[11] M.D. Resh, Fatty acylation of proteins: new insights into membrane targeting of myristoylated and palmitoylated proteins, Biochim. Biophys. Acta 1451 (1999) 1–16.
[12] J. Van Galen, B.W. Van Balkom, R.L. Serrano, D. Kaloyanova, R. Eerland, E. Stueven, J.B. Helms, Binding of GAPR-1 to negatively charged phospholipid membranes: unusual binding characteristics to phosphatidylinositol, Mol. Membr. Biol. 27 (2010) 81–91.
[13] M.R. Macbeth, H.L. Schubert, A.P. Vandemark, A.T. Lingam, C.P. Hill, B.L. Bass, Inositol hexakisphosphate is bound in the ADAR2 core and required for RNA editing, Science 309 (2005) 1534–1539.
[14] J. Reineke, S. Tenzer, M. Rupnik, A. Koschinski, O. Hasselmayer, A. Schrattenholz, H. Schild, C. von Eichel-Streiber, Autocatalytic cleavage of *Clostridium difficile* toxin B, Nature 446 (2007) 415–419.
[15] X. Tan, L.I. Calderon-Villalobos, M. Sharon, C. Zheng, C.V. Robinson, M. Estelle, N. Zheng, Mechanism of auxin perception by the TIR1 ubiquitin ligase, Nature 446 (2007) 640–645.
[16] S.A. Datta, Z. Zhao, P.K. Clark, S. Tarasov, J.N. Alexandratos, S.J. Campbell, M. Kvaratskhelia, J. Lebowitz, A. Rein, Interactions between HIV-1 Gag molecules in solution: an inositol phosphate-mediated switch, J. Mol. Biol. 365 (2007) 799–811.
[17] S.K. Milano, Y.M. Kim, F.P. Stefano, J.L. Benovic, C. Brenner, Nonvisual arrestin oligomerization and cellular localization are regulated by inositol hexakisphosphate binding, J. Biol. Chem. 281 (2006) 9812–9823.
[18] M.R. Groves, A. Kuhn, A. Hendricks, S. Radke, R.L. Serrano, J.B. Helms, I. Sinning, Crystallization of a Golgi-associated PR-1-related protein (GAPR-1) that localizes to lipid-enriched microdomains, Acta Crystallogr. D Biol. Crystallogr. 60 (2004) 730–732.
[19] CCP4, The CCP4 suite: programs for protein crystallography, Acta Crystallogr. D Biol. Crystallogr. 50 (1994) 760–763.
[20] A.J. McCoy, R.W. Grosse-Kunstleve, P.D. Adams, M.D. Winn, L.C. Storoni, R.J. Read, Phaser crystallographic software, J. Appl. Crystallogr. 40 (2007) 658–674.
[21] P. Emsley, K. Cowtan, Coot: model-building tools for molecular graphics, Acta Crystallogr. D Biol. Crystallogr. 60 (2004) 2126–2132.
[22] G. Rouser, A.N. Siakotos, S. Fleischer, Quantitative analysis of phospholipids by thin-layer chromatography and phosphorus analysis of spots, Lipids 1 (1966) 85–86.
[23] A.D. Bangham, J. De Gier, G.D. Greville, Osmotic properties and water permeability of phospholipid liquid crystals, Chem. Phys. Lipids 1 (1967) 225–246.
[24] F.H. Tsao, Purification and characterization of two rabbit lung Ca2(+)-dependent phospholipid-binding proteins, Biochim. Biophys. Acta 1045 (1990) 29–39.
[25] E.N.M. Nolte-'t Hoen, E.J. Van der Vlist, M. Aalberts, H.C.H. Mertens, B.J. Bosch, W. Bartelink, E. Mastrobattista, E.V.B. van Gaal, W. Stoorvogel, G.J.A. Arkesteijn, M.H.M. Wauben, Quantitative and qualitative flow cytometric analysis of nanosized cell-derived membrane vesicles Nanomedicine: NBM (in press).
[26] E. Krissinel, K. Henrick, Inference of macromolecular assemblies from crystalline state, J. Mol. Biol. 372 (2007) 774–797.
[27] E. Posse, B.F. De Arcuri, R.D. Morero, Lysozyme interactions with phospholipid vesicles: relationships with fusion and release of aqueous content, Biochim. Biophys. Acta 1193 (1994) 101–106.
[28] P.J. French, C.M. Bunce, L.R. Stephens, J.M. Lord, F.M. McConnell, G. Brown, J.A. Creba, R.H. Michell, Changes in the levels of inositol lipids and phosphates during the differentiation of HL60 promyelocytic cells towards neutrophils or monocytes, Proc. Biol. Sci. 245 (1991) 193–201.
[29] C.M. Bunce, P.J. French, P. Allen, J.C. Mountford, B. Moor, M.F. Greaves, R.H. Michell, G. Brown, Comparison of the levels of inositol metabolites in transformed haemopoietic cells and their normal counterparts, Biochem. J. 289 (1993) 667–673.
[30] B.S. Szwergold, R.A. Graham, T.R. Brown, Observation of inositol pentakis- and hexakis-phosphates in mammalian tissues by 31P NMR, Biochem. Biophys. Res. Commun. 149 (1987) 874–881.
[31] S. McLaughlin, A. Aderem, The myristoyl-electrostatic switch: a modulator of reversible protein–membrane interactions, Trends Biochem. Sci. 20 (1995) 272–276.